Design and Implementation of a Novel Approach for Maximum Power Point Tracking

Karim Dahech*‡, Moez Allouche*, Tarak Damak*, Driss Mehdi**

*Laboratory of Sciences and Techniques of Automatic Control and Computer Engineering (Lab-STA), National School of Engineering of Sfax (ENIS), University of Sfax. Postal Box 1173, 3038 Sfax, Tunisia.

**Laboratory of Computer and Automatic for System (LIAS), Poitiers National School of Engineering (ENSIP), University of Poitiers, France

(dahechkarim@yahoo.fr, moez_allouche@yahoo.fr, tarak.damak@enis.rnu.tn, Driss.Mehdi@univ-poitiers.fr)

‡Corresponding Author; Karim Dahech, Postal Box 1173, 3038 Sfax, Tunisia, Tel: +216 97053847, Fax: +216 74275595,dahechkarim@yahoo.fr

Received: 21.12.2017 Accepted:25.02.2018

Abstract- This paper deals with the design, the analysis and the implementation of an integral terminal sliding mode controller. Such a controller is developed to track the peak power of a photovoltaic (PV) system. The selected nonlinear sliding surface is based on the derivative of the PV power with respect to the PV voltage. In addition, the development of the control law does not require the knowledge of the PV voltage or current reference which makes implement action simple. Experimental tests are carried out to demonstrate the efficiency of the proposed scheme. The main advantages of the proposed method can be summarized as: high accuracy or equivalently low steady state tracking error, fast response, simple control law, low complexity and implementation cost. Also, the obtained results show that the designed sliding mode controller is robust to environmental changes.

Keywords- PV system; integral terminal sliding mode control; DC-DC boost converter; maximum power point tracking; Dspace 1104

1. Introduction

Energy demand is continuously increasing as a result of the development of industry, transport and demographic growth throughout the world. According to the majority of forecasters, commercial primary energy consumption is expected to double by 2030 and then triple by 2050. Thus, the production of energy is a central issue in our society with repercussions at all levels (economic, environmental, social ...).

Today, global energy production is based on more than 85% of fissile energies (oil, coal, natural gas, uranium...). However, these are available in limited quantities and their depletion times are estimated to be few decades. In addition, the burning of fossil fuels causes an increase in greenhouse gas emissions that confronts the planet to global warming.

The use of renewable energies for the production of electric power is an adequate solution to overcome the aforementioned disadvantages. Especially, photovoltaic energy, based on the direct conversion of light energy from the sun into electricity, is distinguished from other renewable energies by its significant energy potential. Furthermore, photovoltaic systems require little maintenance, are reliable, adjustable, non-polluting and silent. This energy is increasingly applied in various fields such as irrigation, public lighting and industrial or commercial facilities.

To be used in a wide range of applications and to meet the economic constraints, the conversion chain of these energies must be robust and reliable, but also must have a high efficiency at a low cost. For this, we must extract a maximum power from the renewable source. This is possible if the renewable source works at its maximal power all the time. However, the maximum power point (MPP) varies according to several parameters such as the solar irradiation, the temperature and the nature of the load for the PV system.

Various studies have addressed the problem of searching the operating point to get the maximum energy from the PV modules using different methods to ensure the tracking of the maximum power point. However, the nonlinearity of the PV modules current-voltage characteristic and their dependency on temperature and irradiation make the implementation of these methods very complex. If the transfer of power between the renewable energy sources and the load is not optimal, the overall system efficiency will be greatly

affected. The literature on maximum power point tracking (MPPT) shows a variety of approaches. Several reviews [1-15] on MPPT algorithms for PV system are available including both uniform and partial shading irradiation. These algorithms are analyzed and compared according to the tracking ability under environmental changes, the design and implementation difficulty, the precision, cost and the convergence speed. However, MPPT methods can be categorized as two-stages control methods (Fig.1) and one-stage control methods (Fig.2). For the two stages methods, a first step is used to determine the reference voltage or current of the PV array using, for example, adaptive extremum seeking algorithm [16], incremental conductance method [17], incremental resistance method [18] and artificial neural network method [19]. The second step is to regulate the output PV array voltage or current to the obtained reference point by means of a suitable control law [17; 20; 21]. The main disadvantage of this category is that the interaction between the two stages should be treated properly. For the one stage methods [22; 23], the development of the controller does not require knowledge of reference voltage or current. Consequently, their complexity of design and implementation is relatively low compared to the two stages control methods. Recently, several authors [24-27] have proposed different MPPT approaches based on the sliding mode theory. The selection of the sliding surface is based on the relationship $dP_{PV}/dV_{PV}=0$ or $dP_{PV}/dI_{PV}=0$. In [20], a new strategy is proposed which reduces the requirement of voltage sensors. A new sliding mode controller for grid-connected PV systems is proposed in [26]. This control system is based on the one-loop method. However, its chattering problem increases the voltage ripple of the PV module. Although these approaches are robust to environment changes and load variations, these controllers are not robust to system uncertainties. The results obtained by [26] suggest that the system state reaches the surface and produces a maximum power output persistently.

This paper presents a one-stage integral terminal sliding mode controller for maximum power point tracking. The development of such a controller is performed by selecting a nonlinear sliding surface based on the equation. The organization of the paper is as follows. Section 2 provides the structure and the mathematical model of the studied PV system. The design and the analysis of the integral terminal sliding mode controller are the aims of section 3. Experiment results are given in section 4. Finally, conclusions end the paper.

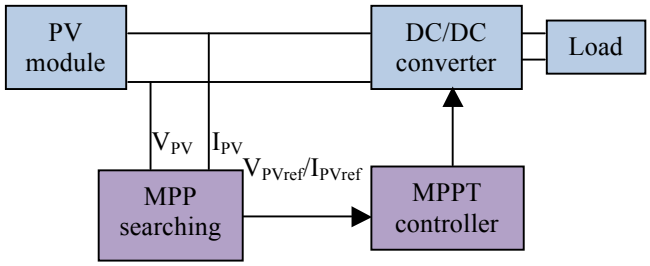

Fig. 1. Two-stages control method.

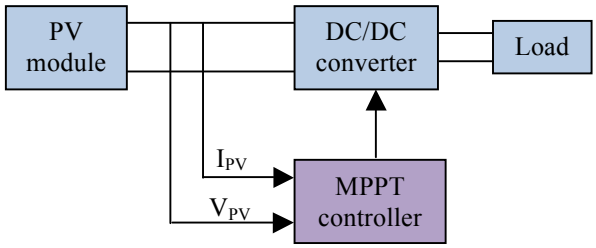

Fig. 2. One-stage control method.

2. System Description and Modeling

Figure 3 shows the structure of the PV system studied in this work. This dispositive is composed of a PV generator, a DC/DC boost converter and a resistive load.

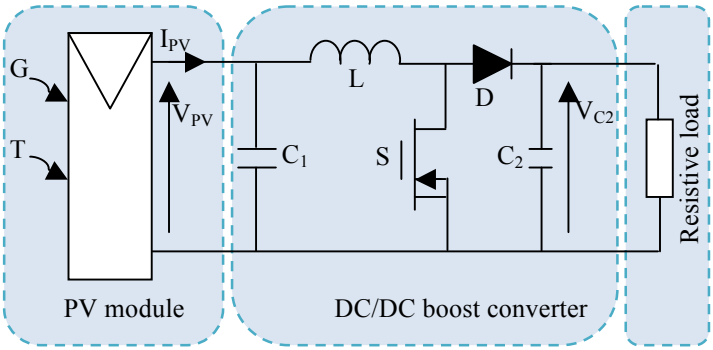

Fig. 3. Photovoltaic system diagram.

2.1. Photovoltaic generator model

A PV module converts light energy into electrical energy. Its mathematical model is based on that of a solar cell since it is composed by a set of cells associated in series and/or parallel. The simplified nonlinear current-voltage characteristic of a PV module is governed by the following equations (1)-(3) [24].

$$I_{PV} = N_p I_{ph} - N_p I_0 \left(e^{\frac{qV_{PV}}{N_s A K_0 T}} - 1 \right) \quad (1)$$

$$I_{ph} = \left(I_{sc} + K_i \left(T - T_{ref} \right) \right) \left(\frac{G}{1000} \right) \quad (2)$$

$$I_0 = I_{0r} \left(\frac{T}{T_{ref}} \right)^3 e^{\frac{qE_g}{K_0 A}\left[1/T_{ref} - 1/T\right]} \quad (3)$$

Where I_{PV} and V_{PV} are the PV module output current and voltage, respectively. N_s and N_p are the numbers of the series and parallel cells, respectively. I_{ph} and I_0 denote the light generated current and the reverse saturation current, respectively. q= 1.60217*10^{-19}C is the electron charge, A is the ideality factor, K_0=1.38*10^{-23}J/K represents the Boltzmann's constant, T denotes the temperature of the photovoltaic module, I_{sc} is the short-circuit cell current under reference conditions, K_i designates the short-circuit

temperature coefficient, G is the solar irradiance, I_{0r} denotes the saturation current at reference temperature T_{ref} and E_g=1.1 ev represents the semiconductor band-gap energy. In this work, the multicrystalline photovoltaic module BP Solar MSX 60 is adopted. Its technical specifications are grouped in table 1. The module is made of 36 multicrystalline silicon solar cells configured as two 18 cell series strings.

Table 1. BP Solar MSX 60 specifications.

Parameter	Value
Maximum power P_{mpp}	60[W]
Short circuit current I_{sc}	3.8[A]
Open circuit voltage V_{oc}	21.1[V]
Maximum voltage V_{mpp}	17.1[V]
Maximum current I_{mpp}	3.5[A]
Temperature coefficient of short circuit current K_i	6.5[mA/°C]
P-N junction characteristic factor A	1.8

2.2. DC/DC boost converter

The structure of the adopted DC/DC converter (Figure 3) is made up of an inductor L, two capacitors (C_1, C_2) and two switches (S, D). According to the state of S, two distinct operating phases of the converter can be distinguished. When the switch S is closed (ON) and the switch D is open (OFF), the current flowing through the inductance will increase linearly and an energy is stored in L. The capacitor C_2 supplies energy to the load. When the switch S is open (OFF) and the switch D is closed (ON), the energy stored in the inductance is transmitted to the capacitor and to the load. Applying Kirchoff's laws to the two above mentioned operating phases and using time average method, the dynamic behavior of the DC/DC boost converter is written as [20]:

$$\begin{aligned}\frac{dV_{pv}}{dt} &= \frac{1}{C_1}\left(I_{pv}-I_L\right)\\ \frac{dI_L}{dt} &= f_1(x)+g_1(x)u(t)\\ \frac{dV_{C2}}{dt} &= f_2(x)+g_2(x)u(t)\end{aligned} \tag{4}$$

Where:

$$f_1(x)=\frac{V_{pv}}{L}-\frac{R_c}{L\left(1+\frac{R_c}{R}\right)}I_L + \frac{1}{L}\left(\frac{R_c}{R+R_c}-1\right)V_{C2}-\frac{V_D}{L} \tag{5}$$

$$g_1(x)=\frac{R_c}{L\left(1+\frac{R_c}{R}\right)}I_L-\frac{1}{L}\left(\frac{R_c}{R+R_c}-1\right)V_{C2}+\frac{V_D}{L} \tag{6}$$

$$f_2(x)=\frac{1}{C_2\left(1+\frac{R_c}{R}\right)}I_L+\frac{1}{C_2\left(R+R_c\right)}V_{C2} \tag{7}$$

$$g_2(x)=-\frac{1}{C_2\left(1+\frac{R_c}{R}\right)}I_L \tag{8}$$

In the next section, an integral terminal sliding mode controller is presented to track the maximum power point of a photovoltaic system.

3. Integral Terminal Sliding Mode Control

Sliding mode control is robust to uncertainties and parametric variations. It is also simple to implement. The design of such a controller has two stages. In the first step, a sliding surface is chosen based on the control aims. In the second step, a control law is developed to fulfill some conditions. The sliding surface is adopted based on the equation (9)

$$y=\frac{dP_{PV}}{dV_{PV}}=\frac{d}{dV_{PV}}\left(V_{PV}\cdot I_{PV}\right)=I_{PV}+V_{PV}\frac{dI_{PV}}{dV_{PV}} \tag{9}$$

Equation (9) can be written in another way as follows:

$$y=I_{PV}+V_{PV}\frac{dI_{PV}/dt}{dV_{PV}/dt}=I_{PV}\frac{dV_{PV}}{dt}+V_{PV}\frac{dI_{PV}}{dt} \tag{10}$$

For the integral terminal sliding mode controller, the following sliding surface σ is adopted:

$$\sigma=y+\alpha\int_0^t y^{p/q}(\tau)d(\tau) \tag{11}$$

Where α is a positive constant and $p,q>0$ are odd integers.

Deriving σ with respect to time, we obtain:

$$\begin{aligned}\frac{d\sigma}{dt} &= \frac{dy}{dt}+\alpha y^{p/q}\\ &= I_{PV}\frac{d^2V_{PV}}{dt^2}+V_{PV}\frac{d^2I_{PV}}{dt^2}+2\frac{dV_{PV}}{dt}\frac{dI_{PV}}{dt}+\alpha y^{p/q}\end{aligned} \tag{12}$$

Since, $I_{PV} = I_{ph} - I_0\left(e^{AV_{PV}} - 1\right)$, the following equations are obtained:

$$\frac{dI_{PV}}{dt} = \frac{dI_{ph}}{dt} + \Upsilon\frac{dV_{PV}}{dt} \tag{13}$$

$$\frac{d^2I_{PV}}{dt^2} = \frac{d^2I_{ph}}{dt^2} + \Upsilon\frac{d^2V_{PV}}{dt^2} + A\Upsilon\left(\frac{dV_{PV}}{dt}\right)^2 \tag{14}$$

$$\frac{d^2V_{PV}}{dt^2} = \frac{1}{C_1}\left(\frac{dI_{ph}}{dt} + \Upsilon\frac{dV_{PV}}{dt} - \frac{dI_L}{dt}\right) \tag{15}$$

Where: $\Upsilon = -AI_0e^{AV_{PV}}$

Insertion of Eq.(13), Eq.(14) and Eq.(15) into Eq.(12) yields:

$$\frac{d\sigma}{dt} = F(x) + G(x)u \tag{16}$$

Where:

$$\begin{aligned} F(x) = &\left(\frac{I_{PV} + \Upsilon V_{PV}}{C_1}\right)\left(\frac{dI_{ph}}{dt} + \Upsilon\frac{dV_{PV}}{dt} - f_1(x)\right) \\ &+ V_{PV}\frac{d^2I_{ph}}{dt^2} + 2\frac{dV_{PV}}{dt}\frac{dI_{ph}}{dt} \\ &+ \left(\frac{dV_{PV}}{dt}\right)^2\left(2\Upsilon + A\Upsilon V_{PV}\right) \end{aligned} \tag{17}$$

$$G(x) = -g_1(x)\left(\frac{I_{PV} + \Upsilon V_{PV}}{C_1}\right) \tag{18}$$

The formulation of a sliding mode controller must accomplish three conditions to ensure stability and sufficient performances which are transversality, equivalent control and reachability [25].

3.1. Transversality condition

The transversality evaluates the controllability of the system. To guarantee the capability of the controller to modify the system dynamics, the transversality condition Eq.(19) has to be ensured.

$$\frac{d}{du}\left(\frac{d\sigma}{dt}\right) \neq 0 \tag{19}$$

When deriving Eq.(16) with respect to u, we obtain:

$$\frac{d}{du}\left(\frac{d\sigma}{dt}\right) = -g_1(x)\left(\frac{I_{PV} + \Upsilon V_{PV}}{C_1}\right) \neq 0 \tag{20}$$

Subsequently, the transversality condition is accomplished if $I_{PV} + \Upsilon V_{PV} \neq 0$,since $g_1(x)/C_1 \neq 0$. In other way we have,

$$\begin{aligned} I_{PV} + \Upsilon V_{PV} &= I_{PV} - AI_0e^{AV_{PV}}V_{PV} \\ &= I_{PV} + V_{PV}\frac{dI_{PV}}{dV_{PV}} = \frac{dP_{PV}}{dV_{PV}} \end{aligned} \tag{21}$$

It follows from Eq.(21) that the condition $I_{PV} + \Upsilon V_{PV} \neq 0$ can be hold for $V_{PV} \neq V_{MPP}$. From this, we can deduce that the sliding mode controller is able to bring the photovoltaic system to its MPP.

3.2. Equivalent control condition

Equivalent control condition analyzes the capacity of the system to stay inside the sliding surface σ. Its requires that the smooth feedback u_{eq} of the discontinuous controller u is constrained within the operational limits. For a DC/DC converter, operational limits are 0 and 1. Therefore, the equivalent control condition is given by:

$$\frac{d\sigma}{dt} = 0 \quad \rightarrow \quad 0 < u_{eq} < 1 \tag{22}$$

Replacing u by u_{eq} in Eq.(16) and resolving $\frac{d\sigma}{dt} = 0$ gives:

$$u_{eq} = -\frac{F(x)}{G(x)} \tag{23}$$

After, inserting Eq.(23) in Eq.(22), the following inequality is obtained

$$0 < u_{eq} = -\frac{F(x)}{G(x)} < 1 \tag{24}$$

According to [26], we can use $\frac{dI_{ph}}{dt} = 0$ to simplify the analysis of equation (24). Also, at the maximum power point we have $\frac{dV_{PV}}{dt} = 0$ since the PV module current I_{PV} is equal to the inductance current I_L . Then, replacing $\frac{dV_{PV}}{dt}$ and $\frac{dI_{ph}}{dt}$ by zero into equation (24) yields:

$$0 < u_{eq} = -\frac{f_1(x)}{g_1(x)} = 1 - \frac{V_{PV}}{L\left(g_1(x)\right)} < 1 \tag{25}$$

Neglecting R_c and V_D gives:

$$0 < u_{eq} = 1 - \frac{V_{PV}}{V_{C2}} < 1 \quad \Rightarrow \quad 0 < V_{PV} < V_{C2} \tag{26}$$

Since the studied PV system includes a DC/DC boost converter, the condition in Eq.(26) is persistent. As a result, the equivalent control condition is accomplished.

3.3. Reachability conditions

The reachability conditions analyzes the capability of the system to achieve the sliding surface $\sigma = 0$, which must be fulfilled by appropriate switchings. According to [26], the sign of the transversality condition imposes the value of u for each reachability condition.

As shown in Fig.4, tow cases can be distinguished:

- If $V_{PV} < V_{MPP}$, then $\frac{dP_{PV}}{dV_{PV}} > 0$ and the transversality expression Eq.(20) is negative. Thus, the following reachability conditions must be fulfilled

$$\lim_{\sigma \to 0^-} \frac{d\sigma}{dt}\bigg|_{u=0} > 0 \quad \text{and} \quad \lim_{\sigma \to 0^+} \frac{d\sigma}{dt}\bigg|_{u=1} < 0 \tag{27}$$

- If $V_{PV} > V_{MPP}$ then $\frac{dP_{PV}}{dV_{PV}} < 0$ and the transversality expression Eq.(20) is positive, which imposes the following reachability conditions

$$\lim_{\sigma \to 0^-} \frac{d\sigma}{dt}\bigg|_{u=1} > 0 \quad \text{and} \quad \lim_{\sigma \to 0^+} \frac{d\sigma}{dt}\bigg|_{u=0} < 0 \tag{28}$$

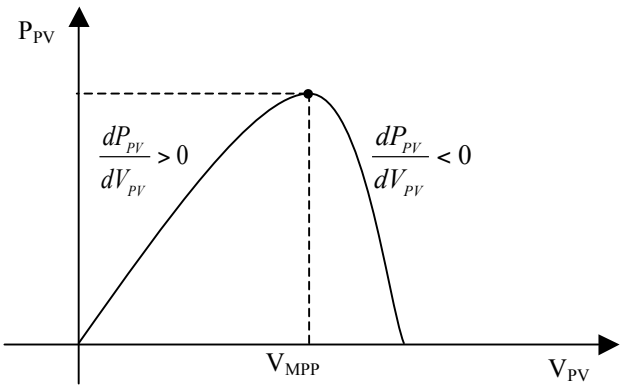

Fig. 4. Sign of dP_{PV}/dV_{PV} at different positions.

3.4. Stability analysis

In order to drive the system to $\sigma = 0$, the control law u is chosen as follows:

$$u = \frac{1}{G(x)}\left[-F(x) - Ksign(\sigma)\right] \tag{29}$$

Where $K > 0$ and $G(x) \neq 0$.

Considering the lyapunov function $V_\sigma = \frac{1}{2}\sigma^2$, the time derivative of V_σ is as follows:

$$\frac{dV_\sigma}{dt} = \sigma \frac{d\sigma}{dt} = \sigma\left(F(x) + G(x)u\right) \tag{30}$$

By substituting Eq.(29) in Eq.(30), we obtain:

$$\frac{dV_\sigma}{dt} < -K|\sigma| \tag{31}$$

Therefore, σ converges to zero at a finite time. As a result, the MPP voltage is reached.

4. Simulation Results

The PV and the associated boost converter together with the integral terminal sliding mode controller have been simulated in MATLAB/Simulink software. The specific solar panel utilized in this research is BP Solar MSX60 PV module. The parameters required to model the PV array were gathered from its manufacturer's data sheet, and are listed in Table 1. The DC/DC boost converter is made up of an inductor $L = 5\,mH$, an input capacitor $C_1 = 500\,\mu F$, an output capacitor $C_2 = 2200\,\mu F$ and a resistive load $R = 20\,\Omega$. The synthesis parameters of the integral terminal sliding mode controller are selected to be $p = 13$, $q = 15$ and $\alpha = 2$.

The proposed method is compared with conventional methods: perturb and observe method (P&O) and incremental conductance (INC) method.

Figures 5 and 6 show the performance comparison of the proposed Integral terminal sliding mode (ITSMC) MPPT with conventional methods (P&O and INC) under a constant cell temperature of 25°C, with solar irradiation (W/m²) changed from 800→1000→800 every 0.2 s. It can be seen from this comparison that the P&O and INC methods are still slower and have larger oscillation compared to the sliding mode control based method.

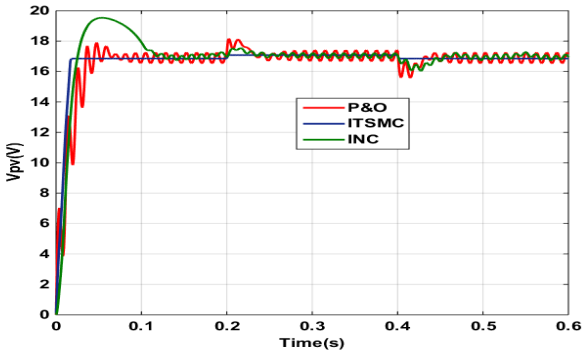

Fig.5. PV module output voltage with ITSMC, P&O and INC methods.

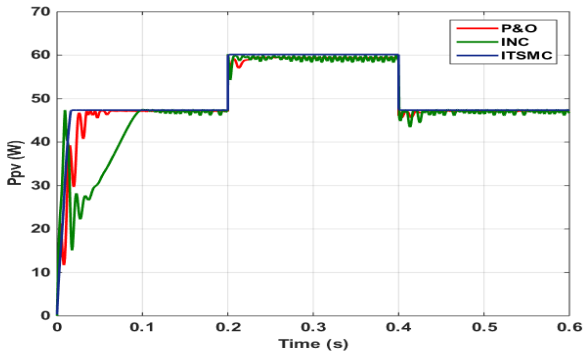

Fig.6. PV module output power with ITSMC, P&O and INC methods.

5. Experiment Results

In order to implement the developed controller, an experimental test bench was designed as shown in Figure 7. The constructed prototype consists of a programmable DC voltage supply (CHROMA 6200H), a DC / DC Boost converter controlled by a Dspace DS1104 real-time card and a resistive load. The programmable DC source operates as a PV emulator instead of solar panels. The DS1104 acquisition card communicates between the system and a computer by using the Matlab / Simulink and Control Desk software tools.

Also, some accessories have been used for measuring and visualization: A LEM PR30 current sensor was used for measuring the output current at the output of the PV emulator; An ST 1000 2-way differential sensor was used to measure the input and output voltages of the converter. The MPPT algorithms was implemented in the DS1104 board to generate the MLI signal which actuates the trigger of the Boost IGBT. A Tektronix oscilloscope is used to visualize the various system variables.

Figure 8 illustrates a synoptic scheme of the experimental prototype. From this figure it can be seen that the sensors measure the current and the voltage at the terminals of the PV source and the voltage of the load. These measurements are used by the MPPT algorithm to generate an MLI signal to control the converter. The developed maximum power point algorithm is performed experimentally. The DC/DC boost converter is made up of an inductor $L = 5\,mH$, an input capacitor $C_1 = 500\,\mu F$, an output capacitor $C_2 = 2200\,\mu F$ and a resistive load $R = 20\,\Omega$. The synthesis parameters of the integral terminal sliding mode controller are selected to be $p = 13$, $q = 15$ and $\alpha = 2$. The converter switching frequency is chosen to be 5 kHz. The photovoltaic system is tested under constant and varying solar irradiation.

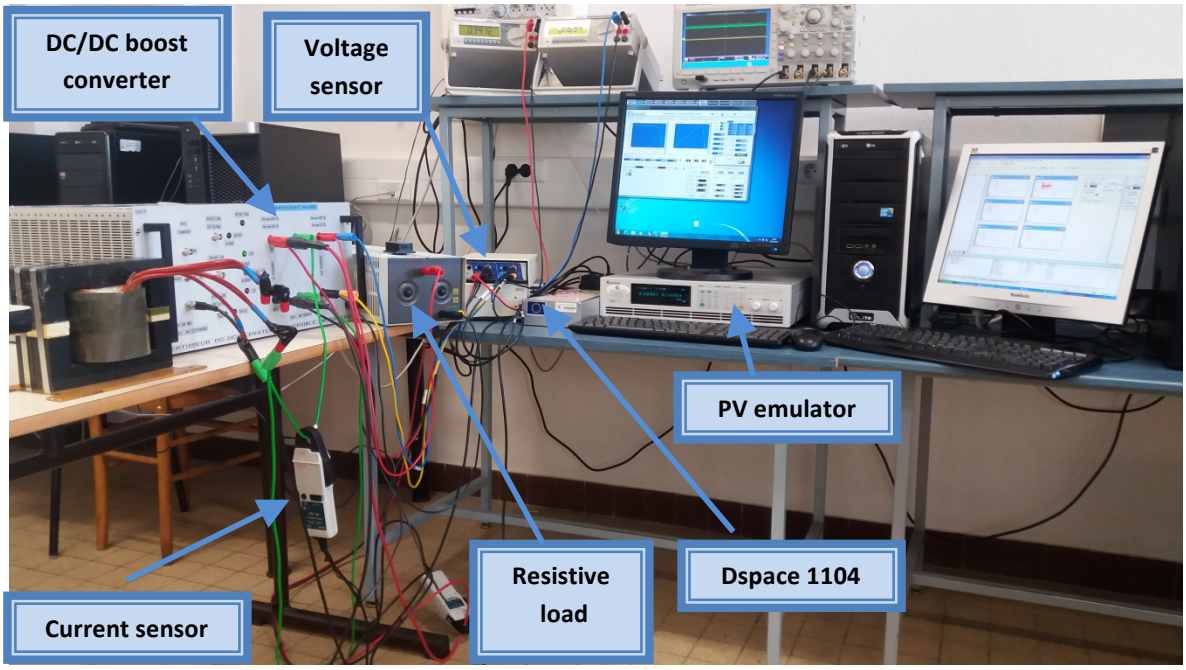

Fig. 7. Experimental test bench diagram.

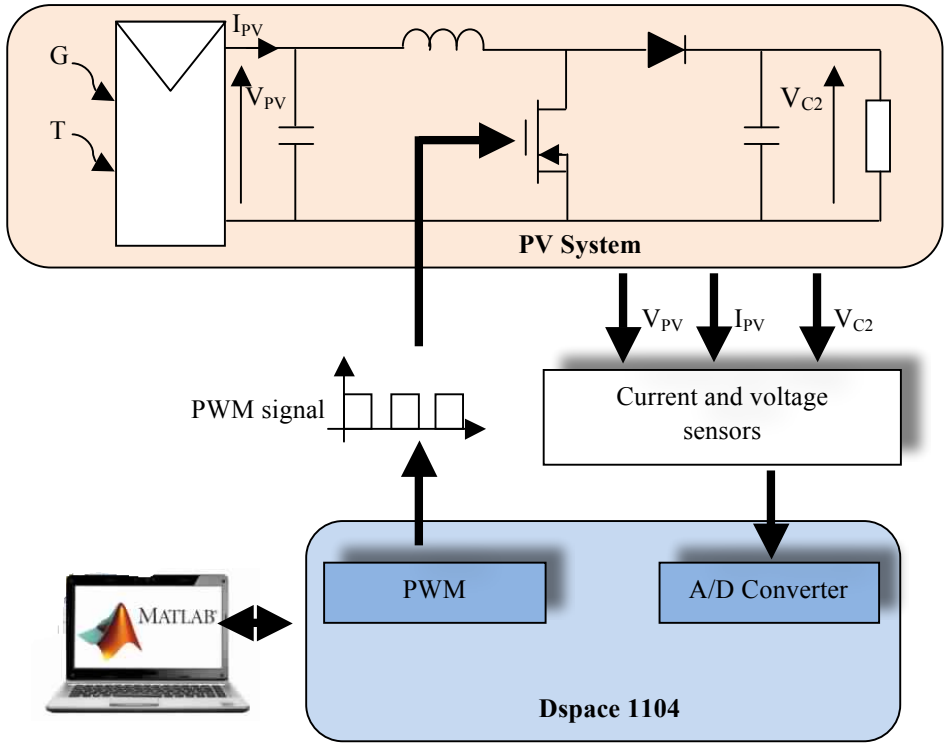

Fig.8. Synoptic scheme of the experimental prototype.

First test: *Constant solar irradiation*

The test is carried out under standard conditions ($G = 1000 W / m^2$ and $T = 25°C$). Figures 9 to 13 depict the real results of the output photovoltaic module voltage, current and power. From these curves, we can see that the proposed algorithm achieves the maximum power point after 0.3 sec. moreover, The steady state is characterized by an accurate and less oscillating behavior. As shown in Fig.12, the duty cycle has a adequate behavior without overshoot. Figure 13 outlines the evolution of the sliding surface which converges to zero when the maximum power is reached.

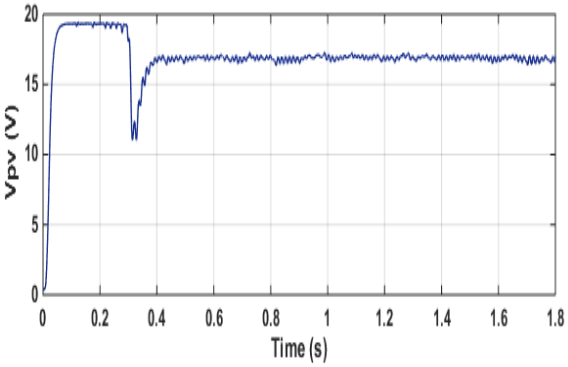

Fig. 9. PV module output voltage under constant radiance.

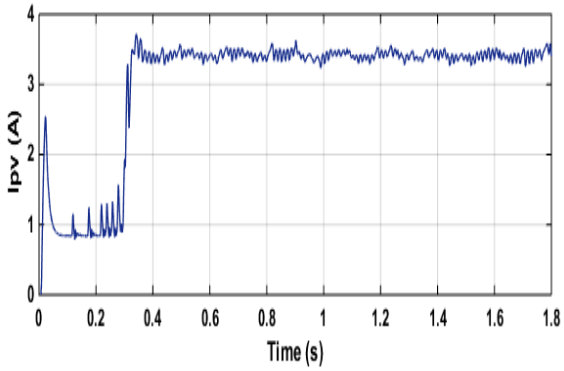

Fig.10. PV module output current under constant radiance.

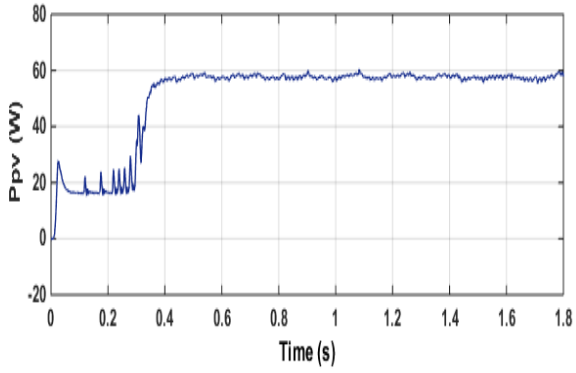

Fig.11. PV module output power under constant radiance.

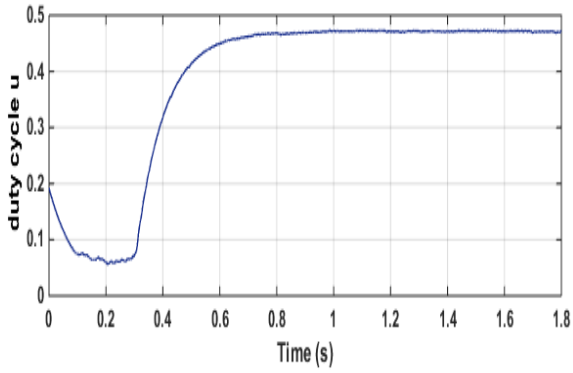

Fig. 12. Duty cycle.

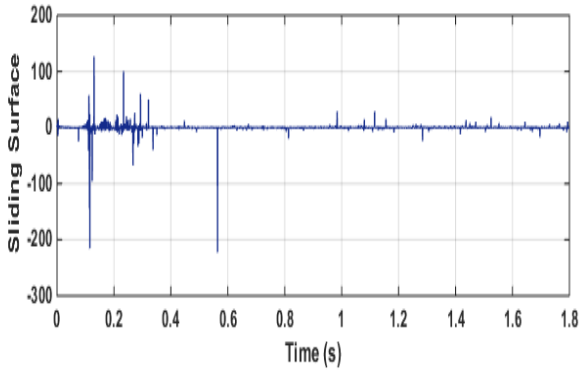

Fig. 13. Sliding surface

Second test: *Varying solar irradiation*

In the second test, the designed control law is tested under solar irradiation changes. Indeed, the irradiance G changes from 800W/m^2 to 1000W/m^2 and then dropped to 800W/m^2. Figures 14 to 18 illustrate the results relative to the application of the developed approach to the designed photovoltaic system. By examinating the different curves, we can confirm the ability of the control law to track the maximum power. Indeed, the PV power reaches the maximum power point with an accurate transient phase, and a low power tracking error is also illustrated. Moreover, the steady state operation is characterized by slight fluctuations.

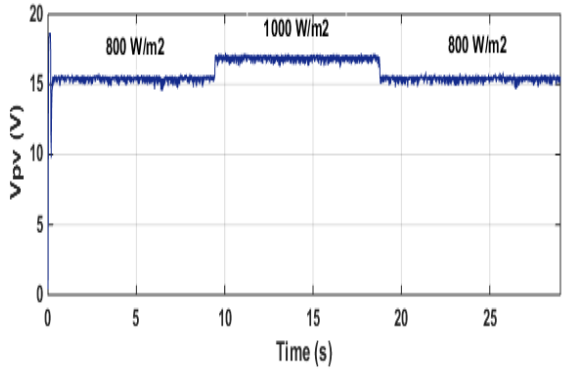

Fig. 14. PV module output voltage under varying radiance.

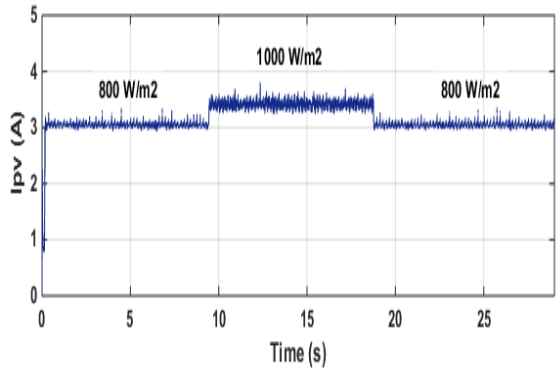

Fig. 15. PV module output current under varying radiance.

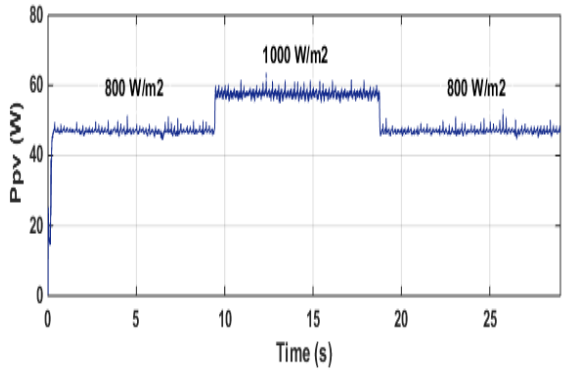

Fig.16. PV module output power under varying radiance.

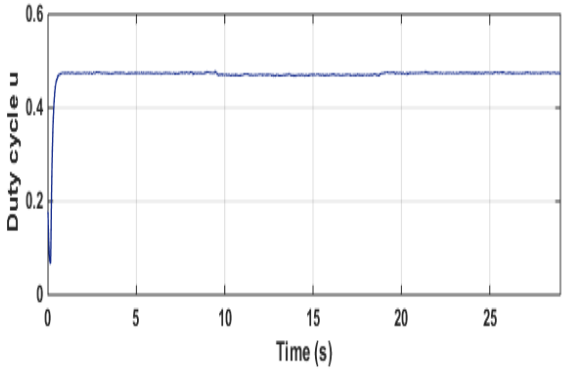

Fig.17. Duty cycle.

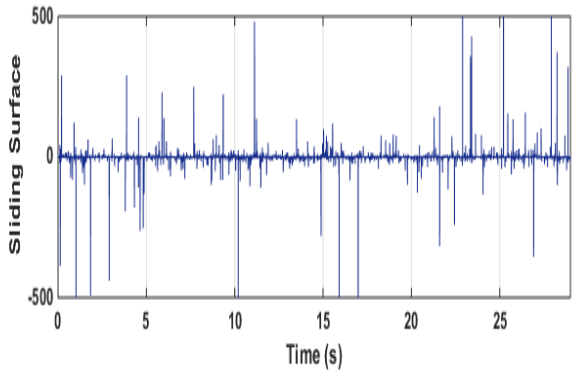

Fig. 18. Sliding Surface.

6. Conclusions

This work illustrates a control approach, based on the variable structure theory, in order to track the maximum power point of a photovoltaic system. The sliding surface was chosen based on the equation $dP_{PV}/dV_{PV} = 0$. Furthermore, the synthesis of the controller does not need the knowledge of the photovoltaic module voltage or current reference. Besides, a comprehensive analysis of the controller is presented. The developed algorithm was validated on an experimental test bench which includes a PV emulator, a DC/DC boost converter, a resistive load, voltage and current sensors and a Dspace DS1104 ensuring the communication between the control and the power parts of the system. The effectiveness of the controller was demonstrated under constant and varying solar irradiation levels. The obtained results confirm that the proposed approach ensures a fast and an accurate tracking of the maximum power point under constant or variable irradiance conditions.

Acknowledgments

This work has been experimentally validated thanks to the experimental test bench in the LIAS-ENSIP laboratory in Univ. Poitiers. The authors would like to thank as well Mr. Driss Mehdi and Mr. Jean Paul Gaubert for helping during the experimental validation of the algorithm.

References

[1] Bhatnagar, P., Nema, R.K., 2013. Maximum power point tracking control techniques: State-of-the-art in photovoltaic applications. Renewable and Sustainable Energy Reviews 23, 224–241.

[2] Reisi, A.R., Moradi, M.H., Jamasb, S., 2013. Classification and comparison of maximum power point tracking techniques for photovoltaic system: A review. Renewable and Sustainable Energy Reviews 19, 433–443.

[3] Salas, V., Olias, E., Barrado, A., Lazaro, A., 2006. Review of the maximum power point tracking algorithms for stand-alone photovoltaic systems. Solar Energy Materials & Solar Cells 90, 1555–1578.

[4] Karami, N., Moubayed, N., Outbib, R., 2017. General review and classification of different MPPT Techniques. Renewable and Sustainable Energy Reviews 68, 1-18.

[5] Verma, D., Shandilya, A.M., Soubhagya, K.D.,2016. Maximum power point tracking (MPPT) techniques: Recapitulation in solar photovoltaic systems. Renewable and Sustainable Energy Reviews 54, 1018-1034.

[6] Bendib, B., Belmili, H., Krim, F., 2015. A survey of the most used MPPT methods: Conventional and advanced algorithms applied for photovoltaic systems. Renewable and Sustainable Energy Reviews 45, 637-648.

[7] Kamarzaman, N.A., Tan, C.W., 2014. A comprehensive review of maximum power point tracking algorithms for photovoltaic systems. Renewable and Sustainable Energy Reviews 37, 585-598.

[8] Liu, Y.H., Chen, J.H., Huang, J.W., 2015. A review of maximum power point tracking techniques for use in partially shaded conditions. Renewable and Sustainable Energy Reviews 41, 436-453.

[9] Ishaque, K., Salam, Z., 2013. A review of maximum power point tracking techniques of PV system for uniform insolation and partial shading condition. Renewable and Sustainable Energy Reviews 19, 475-488.

[10] Zhong, Z.D., Huo, H.B., Zhu, X.J., Cao, G.Y.,Ren, Y., 2008. Adaptive maximum power point tracking control of fuel cell power plants. Journal of Power Sources 176, 259–269.

[12]Dolara, A., Leva, S., Magistrati, G., Mussetta, M., Ogliari, E., Varun Arvind, R., 2016. A novel MPPT algorithm for photovoltic systems under dynamic partial shading recurrent scan and track method. IEEE 5th International Conference on Renewable Energy Research and Application (ICRERA), 1122-1127.

[13] Balaji, V., Amruth, R. T., Ganesan, R., Takaharu, T., 2016. Efficient MPPT control for fast irradiation changes and partial shading conditions on PV systems. IEEE 5th International Conference on Renewable Energy Research and Application (ICRERA), 358-363.

[14] Balaji, V., Wataru, K., Takaharu, T., 2014. MPPT method for PV modules using current control-based partial shading detection. IEEE 3th International Conference on Renewable Energy Research and Application (ICRERA), 359-364.

[15] Boukenoui, R., Bradai, R., Mellit, A., Ghanes, M., Salhi, H., 2015. Comparative analysis of P&O, modified hill climbing-FLC, and adaptive P&O-FLC MPPTs for microgrid standalone PV system. IEEE 4th International Conference on Renewable Energy Research and Application (ICRERA), 1095-1099.

[16] Chian-Song, C., Ya-Lun, O., Chan-Yu, K., 2012. Terminal sliding mode control for maximum power point tracking of photovoltaic power generation systems. Solar Energy 86, 2986–2995.

[17] Dahech, K., Allouche, M., Damak, T., Tadeo, F., 2017. Backstepping sliding mode control for maximum power point tracking of a photovoltaic system. Electric Power Systems Research 143, 182-188.

[18] Zaidi, A., Dahech, K., Damak, T., 2016. Maximum power point tracking of photovoltaic systems based on fast terminal sliding mode controller. International Journal of Renewable Energy Research, 6, 1435-1445.

[19] Mojallizadeh, M.R., Badamchizadeh, M., Khanmohammadi, S., Sabahi, M., 2016. Designing a new robust sliding mode controller for maximum

power point tracking of photovoltaic cells. Solar Energy, 132, 538-546.

[20] Zhang, F., Maddy, J., Premier, G., Guwy, A., 2015. Novel current sensing photovoltaic maximum power point tracking based on sliding mode control strategy. Solar Energy, 118, 80-86.

[21] Chen-Chi C., Chieh-Li, C., 2009. Robust maximum power point tracking method for photovoltaic cells: A sliding mode control approach. Solar Energy, 83, 1370-1378.

[22] Naoufel, K., Youssef, B., Hassan, M., Malika, Z., 2017. Experimental Test Bench of Photovoltaic Systems Using Backstepping MPPT Algorithm. International Journal of Renewable Energy Research, 7, 816-824.

[23] Bharath, K. R., Eenisha, S., 2017. Design and Implementation of Improved Fractional Open Circuit Voltage Based Maximum Power Point Tracking Algorithm for Photovoltaic Applications. International Journal of Renewable Energy Research, 7, 1109-1119.

[24] Yatimi, H., Aroudam, E., 2016. Assessment and control of a photovoltaic energy storage system based on the robust sliding mode MPPT controller. Solar Energy, 139, 557-568.

[25] Montoya, D.G., Ramos-Paja, C.A., Giral, R., 2016. Improved design of sliding-mode controllers based on the requirements of MPPT techniques. IEEE Transactions On Power Electronics, 31, 235-247.

[26] Ortiz Valencia, P.A., Ramos-Paja, C.A., 2015. Sliding-Mode Controller for Maximum Power Point Tracking in Grid-Connected Photovoltaic Systems. Energies, 8, 12363-12387.

[27] Sira-Ramirez, H., 1987. Sliding motions in bilinear switched networks. IEEE Transactions on Circuits and Systems, 34, 919-933.